Biosensors and Bioelectronics 165 (2020) 112287

Contents lists available at ScienceDirect

Biosensors and Bioelectronics

journal homepage: http://www.elsevier.com/locate/bios

A needle-type biofuel cell using enzyme/mediator/carbon nanotube composite fibers for wearable electronics

Sijie Yin [a], Xiaohan Liu [a], Yuka Kobayashi [c], Yuta Nishina [b], Ryo Nakagawa [b], Ryoji Yanai [c], Kazuhiro Kimura [c], Takeo Miyake [a,*]

[a] Graduate School of Information, Production and Systems, Waseda University, 2-7 Hibikino, Wakamatsu, Kitakyushu, Fukuoka, 808-0135, Japan
[b] Graduate School of Natural Science and Technology, Okayama University, Tsushimanaka, Kita, Okayama, 700-8530, Japan
[c] Department of Ophthalmology, Yamaguchi University Graduate School of Medicine Ube, Yamaguchi, 755-8505, Japan

ARTICLE INFO

Keywords:
Enzymatic biofuel cell
Needle-type
Minimal invasive
Power generation biocompatibility

ABSTRACT

To realize direct power generation from biofuels in natural organisms, we demonstrate a needle-type biofuel cell (BFC) using enzyme/mediator/carbon nanotube (CNT) composite fibers with the structure Osmium-based polymer/CNT/glucose oxidase/Os-based polymer/CNT. The composite fibers performed a high current density (10 mA/cm^2) in 5 mM artificial blood glucose. Owing to their hydrophilicity, they also provided sufficient ionic conductivity between the needle-type anode and the gas-diffusion cathode. When the tip of the anodic needle was inserted into natural specimens of grape, kiwifruit, and apple, the assembled BFC generated powers of 55, 44, and 33 μW from glucose, respectively. In addition, the power generated from the blood glucose in mouse heart was 16.3 μW at 0.29 V. The lifetime of the BFC was improved by coating an anti-fouling polymer 2-methacryloyloxyethyl phosphorylcholine (MPC) on the anodic electrode, and sealing the cathodic hydrogel chamber with medical tape to minimize the water evaporation without compromising the oxygen permeability.

1. Introduction

Wearable power sources are key elements in the development of skin electronics (Berchmans et al., 2014; Liu et al., 2017; Pu et al., 2017) and medical devices(Hung et al., 2004; Khan et al., 2016; Wei and Liu 2008). Wearable power sources are designed for continuous contact on the skin surface, where they can harvest energy from the human body. Examples include power generation from the heart (Zurbuchen et al., 2013), mechanical motion (Dagdeviren et al., 2014), and biochemical fuels (Katz et al., 2010). Additionally, as they are worn on the skin, the power sources must be safe and comfortable.

Enzyme-based biofuel cells (BFCs) have attracted much attention as wearable power sources with high power output and guaranteed safety (Cosnier et al., 2016; Haneda et al., 2012; Willner et al., 2009). Two types of BFCs have been developed for wearable applications: i) non-invasive BFCs that directly contact with sweat, tears, and urine, and ii) minimally invasive BFCs that insert miniature needles into skin-covered natural organisms. Prototypes of non-invasive BFCs exist including enzyme-coated carbon fibers woven on textile fabrics (Miyake et al., 2013; Ogawa et al., 2015) and ink-jet-printed cloth (Cheng et al., 2005; Taylor et al., 2007), which harvest energy from lactic acid (Bandodkar et al., 2017; Reid et al., 2015), glucose (Cinquin et al., 2010a; Ivnitski et al., 2006) and ascorbic acid (Goto et al., 2014; Zloczewska et al., 2014) in sweat and tears. Another prototypes is a screen-printed diaper (Shitanda et al., 2019) that utilizes the uric acid in urine. Although the biofuels are produced at sufficiently high concentrations (μM to mM), they are produced at extremely low rates [0.4 μl min^{-1} cm^{-2} from sweat (Vimieiro-Gomes et al., 2005) and 3 μl min^{-1} cm^{-2} from tear (Reid et al., 2015)]. The theoretical maximum power outputs from glucose and lactic acid are only 5.79 μW and 48.24 μW, respectively (Ikeda and Kano 2003).

To overcome the inefficient flow of biofuels into the BFCs, researchers have developed minimally invasive needle BFCs, which directly insert the needle into the skin. Needle-type BFCs are classified into two types: polymeric microneedles (Rasmussen et al., 2012; Valdés-Ramírez et al., 2014) and metallic hollow needle BFCs (Miyake et al., 2011). A polymeric microneedle BFC is inserted approximately 75 μm deep into soft, thin skin under a pressure of 466 MPa (Chua et al., 2013; Donnelly et al., 2011). Recent microneedle-based BFCs have generated mW level power on the skin surface, sufficient for molecular

* Corresponding author.
E-mail address: miyake@waseda.jp (T. Miyake).

https://doi.org/10.1016/j.bios.2020.112287
Received 14 April 2020; Received in revised form 5 May 2020; Accepted 7 May 2020
Available online 12 May 2020

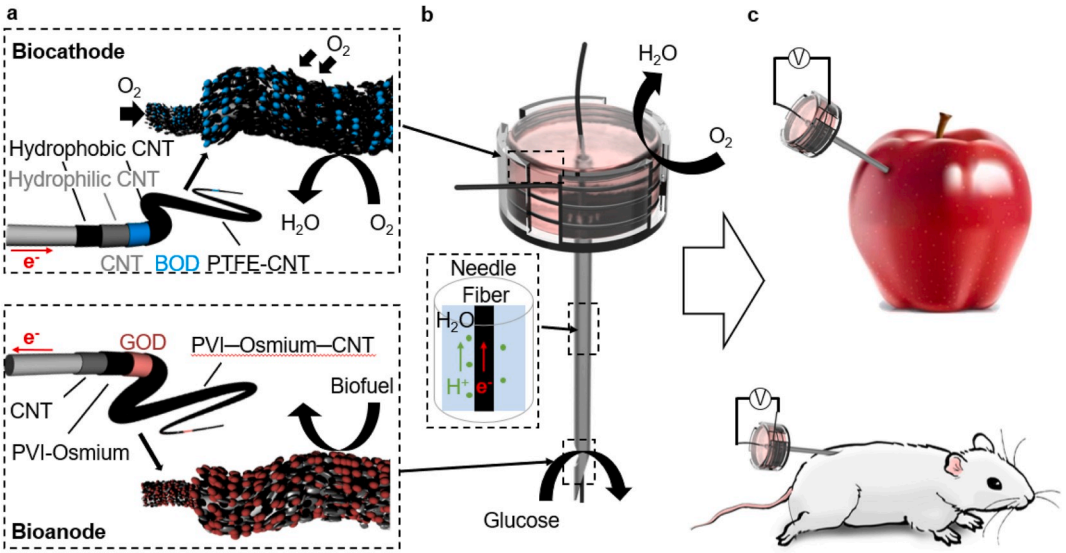

Fig. 1. Schematic of needle-type biofuel cells for direct power generation from glucose in natural organisms. (a) Schemes of oxygen reduction and glucose oxidation at the enzymatic cathode and anode fibers, respectively. (b) The assembled needle cell using the needle anode and the cathode chamber. (c) The assembled cell inserted into an apple and a mouse.

delivery into the skin. Meanwhile, metallic hollow needles are deeply inserted into blood vessels (Cinquin et al., 2010b) or the fleshes of hard-skinned fruits (Slaughter and Kulkarni 2015). Recently, we inserted a needle BFC deeply into a rabbit ear vein and natural grape flesh. The glucose in the vein and fructose in the grape yielded 0.42 μW and 6.3 μW, respectively (Miyake et al., 2011). These devices require high performance of the inserted anodic needle, and high ionic conductivity between the needle-type anode and the cathode.

Here we demonstrate a needle–type BFC based on hydrophilic enzyme/CNT composite fibers, which harvests high power from the glucose in several fruits (grape, apple, and kiwifruit) and in mouse (abdominal cavity and heart) (Fig. 1). The glucose is oxidized by enzyme/mediator/CNT ensemble carbon fibers, which operate through molecular interactions between the π–π stacked CNT and mediator, and through electrostatic interactions between the enzyme and mediator (Fig. 1a). To penetrate the skin barrier in living organisms, we used the metallic-hollow needle filled with enzyme composite fibers. The anode fiber also serves as an ionic conductor between the anodic needle and the cathodic chamber (Fig. 1b). The chamber contains a gas-diffusion biocathode that reduces oxygen from air, and an ion-conducting acrylamide hydrogel (Fig. 1a). The present needle-type BFCs generate power from biochemical sources of glucose biofuel with a single needle insertion (Fig. 1c).

2. Materials and methods

2.1. Materials

Carbon fibers were obtained from FC-R&D Corp (Sagamihara City, Kanagawa, Japan, the diameter of 0.1 mm). The Single-walled carbon nanotubes were purchased from Cheap Tubes. TUBALL single wall carbon nanotube (SWCNT) solution was donated from Kusumoto Chemicals, Ltd (Tokyo, Japan), which is used commonly in commercially-available second battery. Polyvinylimidazole-[Os(bipyridine)$_2$Cl] (PVI-[Os(bpy)$_2$Cl] was donated by Research Core for Interdisciplinary Sciences, Okayama University. Glucose oxidase (GOD, from *Aspergillus sp.*, 100 U mg^{-1} solid), was purchased from Toyobo (Osaka, Japan). Bilirubin oxidase (BOD, from Myrothecium sp.) were purchased from Amano Enzyme Inc. Poly(tetrafluoroethylene) (PTFE) beads were purchased from Sigma-Aldrich. Glucose (99.5%, solid), potassium dihydrogen phosphate (99.0%, solid), dipotassium hydrogen phosphate (99.0%, solid), acrylamide (95.0%, solid), N,N′-methylene-bis(acrylamide) (99.0%, crystal) were purchased from FUJIFILM Wako (Japan). Omnirad 1173 liquid was purchased from Toyotsu Chemiplas Corporation. Injection needles (NN-1838R, 1.2 mm outer diameter) were purchased from TERUMO Corporation, and cotton cord was purchased from Amazon.

2.2. Preparation of bioanode fiber

The GOD-based bioanode for glucose oxidation was fabricated as described in our previous paper (Yin et al., 2019). In our previous works, we used a glucose dehydrogenase (GDH), but the GDH anode require the fuel supplies of both glucose and co-factors. To overcome this drawback, we designed GOD-based anode fibers.

TUBALL SWCNT solution (200 μL) was dropped onto a 10−cm long carbon fiber and dried in an 80 °C oven. After drying, the SWCNT−modified carbon fibers were washed with distilled water to remove the redundant SWCNT. The CNT−coated fibers were soaked in a stirred phosphate buffer solution (PBS, 0.1 M, pH 7.0) containing 1.5 mg/mL PVI-[Os(bpy)$_2$Cl] at 4 °C for 2h. The resulting PVI-Osmium/CNT/fibers were washed in distilled water for 30 min, then immersed in a stirred solution containing 5 mg/mL GOD at 4 °C for 2 h to adsorb the GOD. Finally, the GOD/PVI-[Os(bpy)$_2$Cl]/CNT/fibers were soaked in a stirred 0.2% CNT aqueous solution containing 0.4 mg/ml PVI-[Os(bpy)$_2$Cl] to produce PVI-[Os(bpy)$_2$Cl]−CNT/GOD/PVI-[Os(bpy)$_2$Cl]/CNT/fibers. In the cyclic voltammetry (CV) tests, the current density was measured over a geometric area of 0.09 cm^2.

2.3. Preparation of O_2-diffusion biocathode

The O_2-diffusion biocathode was fabricated as described in our previous paper (Yin et al., 2019). Hydrophobic SWCNT ethanol solution (200 μL, 5.0 mg/mL) containing PTFE particles (1.0 wt%) was dropped onto a 10−cm long carbon fiber and oven−dried three times at 80 °C, yielding a PTFE−CNT layer for O_2 diffusion. The PTFE−CNT/fibers were washed in distilled water for 30 min, then coated with hydrophilic TUBALL CNT to immobilize the BOD enzyme. The CNT/PTFE−CNT/-fibers were soaked in a stirred solution containing 3.0 mg mL^{-1} BOD at 4 °C for 12 h. Another PTFE−CNT layer was coated on the BOD/-CNT/PTFE−CNT/fiber by drop-casting at room temperature. The current density in the CV tests was calculated over a geometric are of 0.18

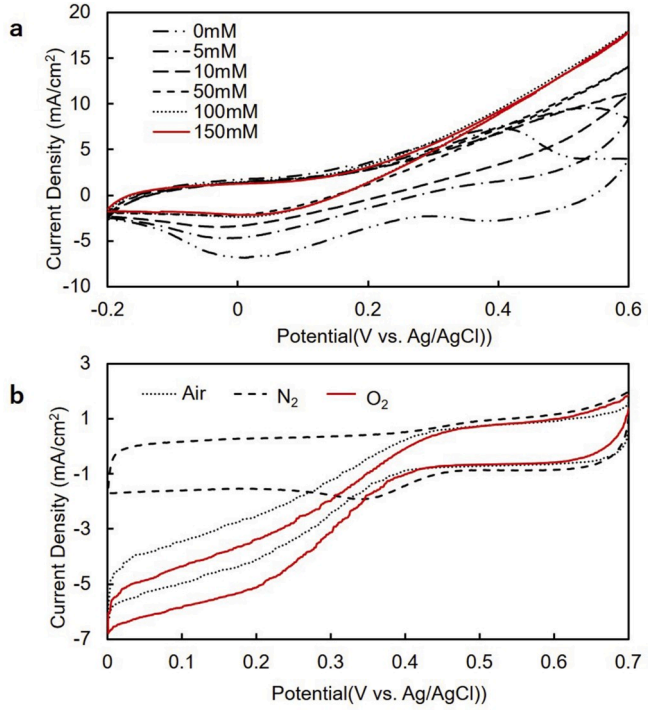

Fig. 2. (a) Cyclic voltammograms of glucose oxidation at 20 mV s^{-1} in buffer solution containing glucose at different concentrations (0–150 mM). (b) Cyclic voltammograms of oxygen reduction at 20 mV s^{-1} in N_2-saturated, air-saturated and O_2-saturated buffer solution.

cm^2.

2.4. Electrochemical measurements

The performances of the enzyme-coated fiber electrodes were analyzed by a three-electrode system (BAS, 2325 model or Hokuto Denko, HSV-110 electrochemical analyzer) in solution using an Ag/AgCl reference electrode and a platinum counter electrode. The GOD-−modified anodes were evaluated in a glucose solution, while the BOD-modified cathodes were evaluated in PBS solution. The performances of the biofuel cells were evaluated by their cell voltages when connected with a variable external resistance (between 100 Ω and 100 kΩ). The current and the power were derived from the cell voltage and resistance. Unless otherwise stated, all data were measured at room temperature (22 °C), and all solutions were based on PBS (pH 7.0).

3. Results and discussion

3.1. Performances of the bioanode and biocathode

The GOD enzyme catalyzes the glucose oxidation by reducing oxygen to water, but this process greatly minimizes the electron transfer from GOD to the collective electrode (Ivnitski et al., 2006). To improve such low electron transfer, we previously applied a PVI–$[Os(bpy)_2Cl]$ mediator on a collective CNT sheet electrode, and achieved a high turnover rate and large catalytic current (Yoshino et al., 2013). The present paper further investigates the performance of GOD-coated composite fibers. The second coating of PVI−$[Os(bpy)_2Cl]$ on the GOD/PVI–$[Os(bpy)_2Cl]$/CNT fibers was expected to increase the amount of PVI–$[Os(bpy)_2Cl]$ around GOD, further improving the turnover rate and enhancing the performance. Here, the PVI–$[Os(bpy)_2Cl]$ concentration was ranged from 0.1 to 0.5 mg/ml in 0.2% CNT aqueous solution (Supporting Fig. 1). The 0.2% CNT solvent was selected to improve the power performance of the electrodes. As the PVI−$[Os(bpy)_2Cl]$ concentration increased from 0 to 0.4 mg/ml, the maximum current density was enhanced from 10 mA/cm^2 (900 μA) to 17.8 mA/cm^2 (1600 μA) in PBS containing 100 mM glucose. Increasing the PVI–$[Os(bpy)_2Cl]$ concentration to 0.5 mg/ml did not raise the current further, implying that 17.8 mA/cm^2 was the saturation current. After determining the optimal method for anode fabrication, we tested the optimized anode PVI–$[Os(bpy)_2Cl]$–CNT/GOD/PVI–$[Os(bpy)_2Cl]$/CNT fibers in PBS containing glucose at different concentrations (Fig. 2a). In the presence of 5 mM glucose [similar to blood glucose levels (Wang 2008)], the oxidation current of the PVI–$[Os(bpy)_2Cl]$–CNT/GOD/PVI–$[Os(bpy)_2Cl]$/CNT was 8.3 mA/cm^2 at 0.6 V. The performance enhanced to 17.8 mA/cm^2 at 100 mM glucose. At higher glucose concentration, the performance was saturated by GOD enzyme activity (Bankar et al., 2009).

To calibrate the performance of the gas-diffusion BOD cathode, we measured the reduction current supplied from oxygen in air. During the measurement, the BOD fibers were partially immersed in solution (10 mm of their length in the solution; 50 mm in air). Because dissolved oxygen has low solubility and a small diffusion coefficient in aqueous solutions (Weiss 1970), highly catalytic BOD cathode requires a

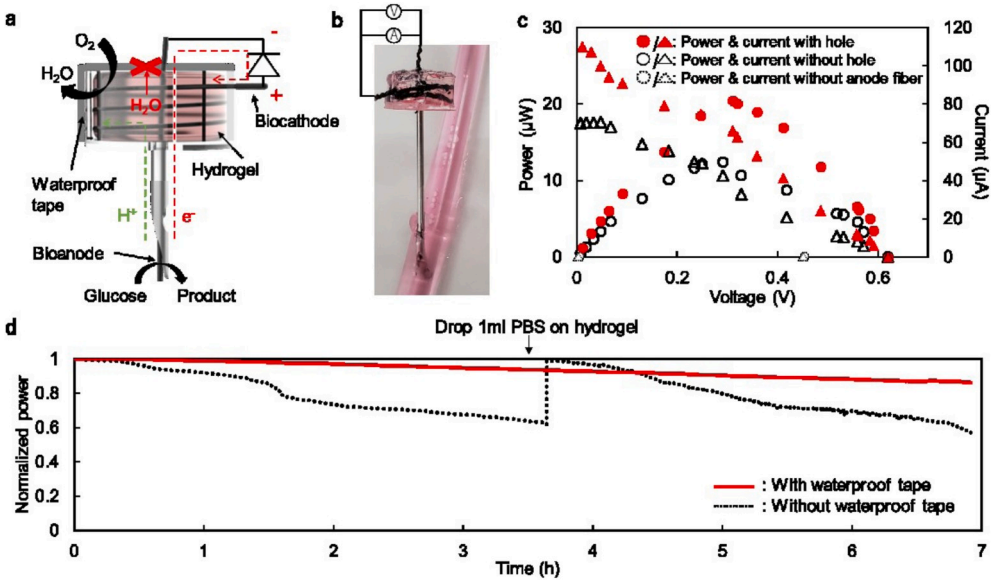

Fig. 3. (a). Schematic of the demonstrated needle-type biofuel cell. (b) Photograph of the needle-type biofuel cell inserted into a mimic blood vessel. (c) Performance of the needle BFC inserted into a mimic blood vessel containing 5 mM glucose. Hollow and solid dashed circles denote the power with and without pores drilled in the wall of the needle (pore area: 10 mm^2). Dashed circles are the results of a control experiment using a metallic hollow needle as the anode. (d) Lifetimes of the needle BFCs with and without the sealing tape. A 1.0 ml aliquot of PBS was dropped on the cathodic chamber of the non-sealed BFC at 3.5 h.

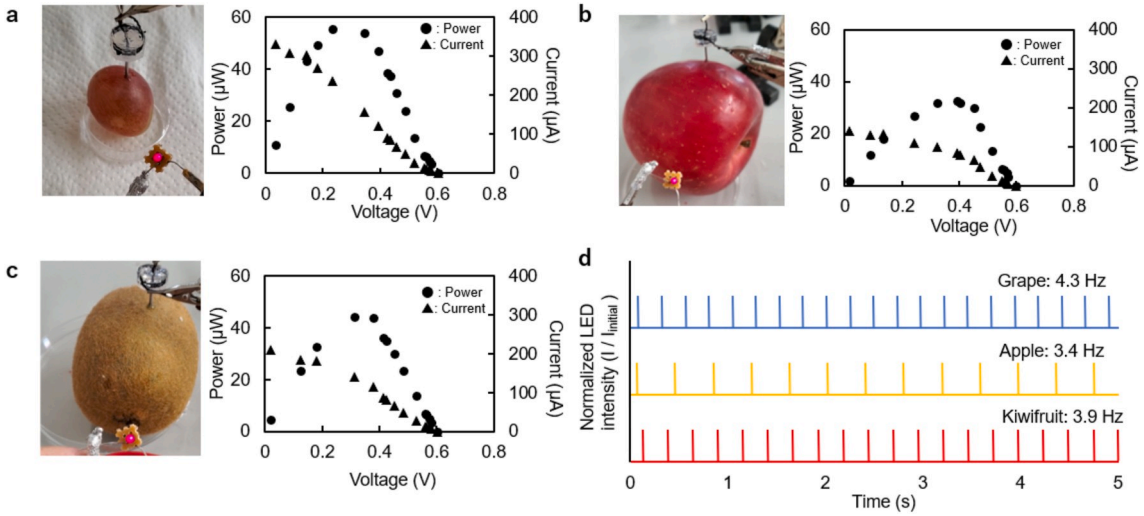

Fig. 4. (a-c) Photographs and performances of the BFC inserted into different fruits: (a)grape, (b) apple, and (c) kiwifruit. (d) LED blinking from the hybrid device (needle BFC combined with an LED system) inserted into grape, apple, and kiwifruit.

gas-diffusion electrode (Haneda et al., 2012). In our previous works (Yin et al., 2019), we found that layered structures of hydrophobic CNT/BOD–hydrophilic CNT/hydrophobic CNT fibers enhanced the oxygen reduction. In this paper, we demonstrate a new type of hydrophilic SWCNT that immobilizes BOD biocatalysts. The reduction current of PTFE–CNT/BOD/SWCNT/PTFE–CNT/fiber in static PBS solution was 6.1 mA/cm^2 at 0V, similar to that obtained under oxygen-rich stirred conditions (6.8 mA/cm^2). In the multilayered structure of BOD composite fibers, an efficient oxygen supply was provided from the air passing through the hydrophobic PTFE–CNT layers; meanwhile, protons were transferred through the hydrophilic SWCNT layer to the BOD catalyst in contact with the fiber.

3.2. Performance of the needle-type BFCs

The needle-type BFC for fruits contained a needled GOD bioanode for glucose oxidation and an oxygen-diffusion BOD cathode (Fig. 3a). Both electrodes were mounted in a plastic chamber (volume = 0.3 ml) filled with acrylamide hydrogel. When the needle tip was inserted into the fruit, the glucose inside the organism was oxidized at the GOD bioanode, while the oxygen from air was reduced to water at the BOD electrode. During these faradaic reactions, the electrons and ions flowed between the anode/cathode through the external electric circuit and the internal ionic conductor, respectively.

Fig. 3c compares the performances of cells using anodic needles with and without side pores. A 10 mm^2 area pore was drilled by a rotary (ARGOFILE Japan) in the sidewall of metallic hollow needles to act as effective windows for fuel supply.

The open-circuit voltage (OCV) of both cells was 0.62 V, the difference between the initial potentials of glucose oxidation and oxygen reduction in the CVs (-0.1 V in Fig. 2a, 0.52 V in Fig. 2b). When the side pores were closed, the maximum power in 5 mM glucose solution was 12.5 μW at 0.29 V (Fig. 3c, hollow circles). Opening the side pores (to 10 mm^2) enhanced the performance to 20.4 μW at 0.31 V (Fig. 3c, solid circles). This improvement was attributed to the high flows of glucose biofuels and gluconic lactone products through the opened apertures in the needle tip. Furthermore, due to the needle was made up with metal, it was necessary to clarify the interference of metal in the anodic reaction. We confirmed no power was generated in a cell containing a BOD cathode and a metallic hollow needle anode without the GOD fiber (Fig. 3c, dashed circles).

The lifetime of the needle BFC was investigated with and without waterproof tape (Fig. 3d). For the lifetime measurements, we connected a 6.8 kΩ resistance between the anode/cathode in the needle BFCs to maximize the power generation, and evaluated the power stability over time. Without the waterproof tape, the power dramatically decreased to 62% of its initial level after 3.5 h. This decrease was attributed to water evaporation from the hydrogel chamber rather than enzyme deactivation. In fact, the power recovered to its original level after dropping 1.0 ml PBS solution on the hydrogel chamber. The evaporation problem was resolved by covering the hydrogel chamber with waterproof tape, which minimized the water loss without compromising the gas permeability. The initial power of the sealed cell was sustained over several hours of operation, and 86% of the initial power remained after continuous operation for 7.0 h (Fig. 3d). By the comparison between with and without waterproof tape, we could conclude the main reason for the power decrement was water evaporation, which indicated that the enzyme could keep a high activity during 7.0 h.

3.3. Power generation from fruits

Power generation by the designed needle BFCs was demonstrated on three different fruits (grape, apple, and kiwifruit). When the BFCs were inserted to a depth of 10 mm into the fruits, their OCVs were consistent (0.62 V), but their power generations were 55 μW, 33 μW, and 44 μW in grape, apple, and kiwifruit, respectively (Fig. 4a–c). Data from "The Paleo Diet" website [https://thepaleodiet.com/fruits-and-sugars/] list the glucose levels in grape, apple, and kiwifruit as 6.5 g, 2.3 g and 5.0 g per 100 g, respectively. Thus, the different cell powers from the fruits were attributed to the different glucose concentrations in the fruits. To monitor these glucose concentrations, we combined the needle BFC with a light-emitting diode (LED) device consisting of a charge pump integrated circuit, a 1.0 μF ceramic capacitor and a red LED. As we described in our previous works (Miyake et al., 2011), the frequency f_{blink} from LED blinking was proportional to the power of the BFC. If this power is wholly supplied by glucose reactions, the glucose concentration in the fruit could be evaluated from f_{blink}. Therefore, before measuring the fruit glucose contents, we calibrated the f_{blink} from LED device in PBS solutions containing different glucose concentrations (1–100 mM). From 1.0 to 10 mM glucose, f_{blink} linearly increased from 2.4 Hz to 5.1 Hz (Supporting Fig. 2). At higher contents, the f_{blink} was saturated by the capacitance limit of the LED device. When inserted into the fruits, the LED device blinked at 4.3 Hz in the grape, 3.4 Hz in the apple, and 3.9 Hz in the kiwifruit. From these f_{blink} values, the glucose concentrations in the grape, apple, and kiwifruit were determined as 7.5, 4.3, and 6.1 mM, respectively. These data well correspond with "The Paleo Diet" data.

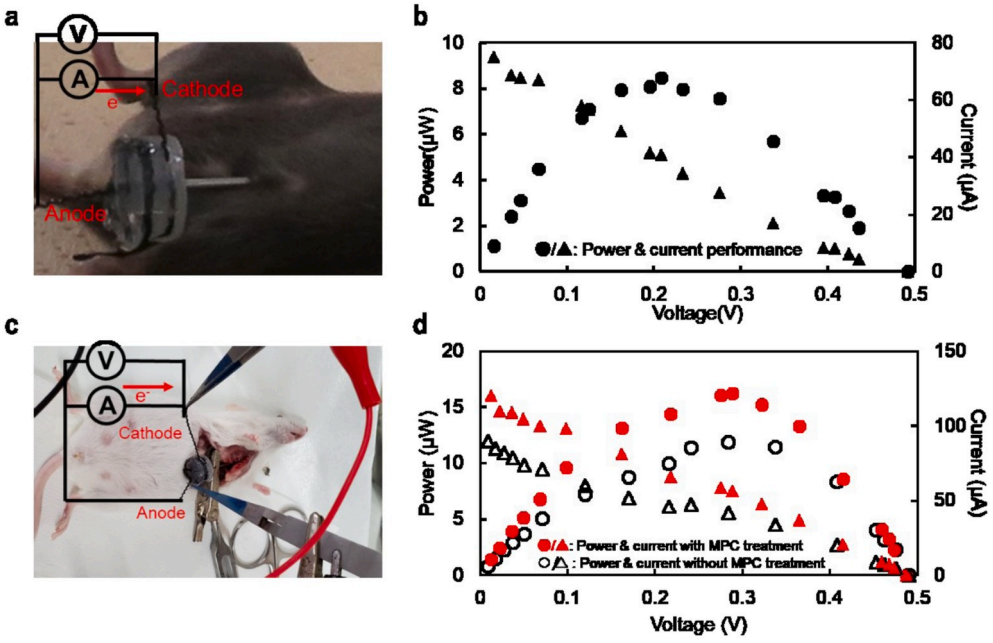

Fig. 5. (a) Photograph of the needle BFC inserted into mouse abdominal cavity. (b) Performance of the BFC in mouse abdominal cavity. (c) Photograph of the needle BFC inserted into mouse heart. (d) Performance of the BFCs with and without MPC coating in mouse heart.

3.4. Power generation from mouse tissue

Similar to the fruit experiments, the needle BFCs were inserted into the abdominal cavities and hearts of female mice (Fig.5a, c). Prior to the needle insertion, the mice were anesthetized with ketamine hydrochloride (35 mg kg^{-1}) and xylazine hydrochloride (5 mg kg^{-1}), and awoke from anesthesia after 1 h. The anesthesia time was sufficient for inserting the cell anode into the abdominal cavity of the mouse and measuring the cell voltage. The OCV of the needle BFCs was 0.5 V in both the abdominal cavity and heart murine tissue (Fig. 5 b, c), lower than in fruits. This result can be explained by the high chloride level of mouse body fluids, which causes a shift of the reduction current from the BOD cathode to a negative potential in the murine tissue (De Poulpiquet et al., 2017).

The BFC power generations from the abdominal cavity and hearts were 8.5 μW at 0.20 V and 11.8 μW, respectively, although the glucose concentrations were almost identical in the cavity (116 mg/dm^3) and the heart (100 mg/dm^3). The probable main reason or the different power generations was the lower volume of interstitial fluid in the abdominal cavity than of blood in the heart. The high fluid volume would increase the internal resistance of the BFC. To improve the power output from heart tissue, we coated an anti-biofouling MPC polymer on both needle tip and anode, as described in our previous paper (Miyake et al., 2011). The MPC polymer improved the maximum power output to 16.3 μW at 0.29 V (Fig. 5d, red dots).

4. Conclusion

A needle-type BFC that harvests the glucose in fruits and mouse and directly converts it to power was developed from composite fibers of enzyme/mediator/CNT. When the tip of the needle-like anode was inserted into grape, kiwifruit, and apple, the needle BFC harvested 55 μW, 44 μW and 33 μW from fruit glucose, respectively. A hybrid BFC-LED device also generated power, and blinked at a frequency that depended on the fruit glucose concentration. The hybrid device was a good demonstration of a self-powered glucose indicator. Furthermore, the needle BFC generated power from the glucose in different locations of murine abdominal cavity (8.5 μW) and heart (16.3 μW) tissue. To improve the power output and lifetime, we coated the anodic needle with an anti-biofouling MPC polymer and sealed the cathodic chamber with waterproof tape. The present harvesting power source can potentially realize wearable electronics inserted into body fluids.

Declaration of competing interest

The authors declare that they have no known competing financial interests or personal relationships that could have appeared to influence the work reported in this paper.

CRediT authorship contribution statement

Sijie Yin: Data curation, Investigation, Writing - original draft, Writing - review & editing. **Xiaohan Liu:** Data curation, Investigation, Writing - original draft, Writing - review & editing. **Yuka Kobayashi:** Data curation, Investigation. **Yuta Nishina:** Investigation, Writing - review & editing. **Ryo Nakagawa:** Investigation. **Ryoji Yanai:** Investigation. **Kazuhiro Kimura:** Investigation. **Takeo Miyake:** Conceptualization, Data curation, Investigation, Writing - review & editing.

Acknowledgements

The research presented in this article was supported by the TEPCO Memorial Foundation. Part of this work was conducted at Kitakyushu Foundation for the Advancement of Industry, Science and Technology, Semiconductor Center, supported by "Nanotechnology Platform Program" of the Ministry of Education, Culture, Sports, Science and Technology (MEXT), Japan.

Appendix A. Supplementary data

Supplementary data to this article can be found online at https://doi.org/10.1016/j.bios.2020.112287.

References

Bandodkar, A.J., You, J.-M., Kim, N.-H., Gu, Y., Kumar, R., Mohan, A.V., Kurniawan, J., Imani, S., Nakagawa, T., Parish, B., 2017. Energy Environ. Sci. 10 (7), 1581–1589.
Bankar, S.B., Bule, M.V., Singhal, R.S., Ananthanarayan, L., 2009. Biotechnol. Adv. 27 (4), 489–501.

Berchmans, S., Bandodkar, A.J., Jia, W., Ramírez, J., Meng, Y.S., Wang, J., 2014. J. Mater. Chem. 2 (38), 15788–15795.
Cheng, K., Yang, M.H., Chiu, W.W., Huang, C.Y., Chang, J., Ying, T.F., Yang, Y., 2005. Macromol. Rapid Commun. 26 (4), 247–264.
Chua, B., Desai, S.P., Tierney, M.J., Tamada, J.A., Jina, A.N., 2013. Sensor Actuator Phys. 203, 373–381.
Cinquin, P., Gondran, C., Giroud, F., Mazabrard, S., Pellissier, A., Boucher, F., Alcaraz, J.-P., Gorgy, K., Lenouvel, F., Mathé, S., 2010a. PloS One 5 (5).
Cinquin, P., Gondran, C., Giroud, F., Mazabrard, S., Pellissier, A., Boucher, F., Alcaraz, J.-P., Gorgy, K., Lenouvel, F., Mathé, S., 2010b. PloS One 5 (5), e10476.
Cosnier, S., Gross, A.J., Le Goff, A., Holzinger, M., 2016. J. Power Sources 325, 252–263.
Dagdeviren, C., Yang, B.D., Su, Y., Tran, P.L., Joe, P., Anderson, E., Xia, J., Doraiswamy, V., Dehdashti, B., Feng, X., 2014. Proc. Natl. Acad. Sci. Unit. States Am. 111 (5), 1927–1932.
De Poulpiquet, A., Kjaergaard, C.H., Rouhana, J., Mazurenko, I., Infossi, P., Gounel, S.b., Gadiou, R., Giudici-Orticoni, M.T.r.s., Solomon, E.I., Mano, N., 2017. ACS Catal. 7 (6), 3916–3923.
Donnelly, R.F., Majithiya, R., Singh, T.R.R., Morrow, D.I., Garland, M.J., Demir, Y.K., Migalska, K., Ryan, E., Gillen, D., Scott, C.J., 2011. Pharmaceut. Res. 28 (1), 41–57.
Goto, H., Fukushi, Y., Nishioka, Y., 2014. In: Journal of Physics: Conference Series. IOP Publishing, 012048.
Haneda, K., Yoshino, S., Ofuji, T., Miyake, T., Nishizawa, M., 2012. Electrochim. Acta 82, 175–178.
Hung, K., Zhang, Y.-T., Tai, B., 2004. In: The 26th Annual International Conference of the IEEE Engineering in Medicine and Biology Society. IEEE, pp. 5384–5387.
Ikeda, T., Kano, K., 2003. Biochim. Biophys. Acta Protein Proteonomics 1647 (1–2), 121–126.
Ivnitski, D., Branch, B., Atanassov, P., Apblett, C., 2006. Electrochem. Commun. 8 (8), 1204–1210.
Katz, E., Shipway, A.N., Willner, I., 2010. Handbook of Fuel Cells.
Khan, Y., Ostfeld, A.E., Lochner, C.M., Pierre, A., Arias, A.C., 2016. Adv. Mater. 28 (22), 4373–4395.
Liu, Y., Pharr, M., Salvatore, G.A., 2017. ACS Nano 11 (10), 9614–9635.
Miyake, T., Haneda, K., Nagai, N., Yatagawa, Y., Onami, H., Yoshino, S., Abe, T., Nishizawa, M., 2011. Energy Environ. Sci. 4 (12), 5008–5012.
Miyake, T., Haneda, K., Yoshino, S., Nishizawa, M., 2013. Biosens. Bioelectron. 40 (1), 45–49.
Ogawa, Y., Takai, Y., Kato, Y., Kai, H., Miyake, T., Nishizawa, M., 2015. Biosens. Bioelectron. 74, 947–952.
Pu, X., Liu, M., Chen, X., Sun, J., Du, C., Zhang, Y., Zhai, J., Hu, W., Wang, Z.L., 2017. Sci. Adv. 3 (5), e1700015.
Rasmussen, M., Ritzmann, R.E., Lee, I., Pollack, A.J., Scherson, D., 2012. J. Am. Chem. Soc. 134 (3), 1458–1460.
Reid, R.C., Minteer, S.D., Gale, B.K., 2015. Biosens. Bioelectron. 68, 142–148.
Shitanda, I., Fujimura, Y., Nohara, S., Hoshi, Y., Itagaki, M., Tsujimura, S., 2019. Based disk-type. J. Electrochem. Soc. 166 (12), B1063.
Slaughter, G., Kulkarni, T., 2015. J. Biochips Tissue Chips 5 (1), 1.
Taylor, A.D., Kim, E.Y., Humes, V.P., Kizuka, J., Thompson, L.T., 2007. J. Power Sources 171 (1), 101–106.
Valdés-Ramírez, G., Li, Y.-C., Kim, J., Jia, W., Bandodkar, A.J., Nuñez-Flores, R., Miller, P.R., Wu, S.-Y., Narayan, R., Windmiller, J.R., 2014. Electrochem. Commun. 47, 58–62.
Vimieiro-Gomes, A., Magalhaes, F., Amorim, F., Machado-Moreira, C., Rosa, M., Lima, N., Rodrigues, L., 2005. Braz. J. Med. Biol. Res. 38 (7), 1133–1139.
Wang, J., 2008. Chem. Rev. 108 (2), 814–825.
Wei, X., Liu, J., 2008. Front. Energy Power Eng. China 2 (1), 1–13.
Weiss, R.F., 1970. Deep Sea Research and Oceanographic Abstracts. Elsevier, pp. 721–735.
Willner, I., Yan, Y.M., Willner, B., Tel-Vered, R., 2009. Fuel Cell. 9 (1), 7–24.
Yin, S., Jin, Z., Miyake, T., 2019. Biosens. Bioelectron. 141, 111471.
Yoshino, S., Miyake, T., Yamada, T., Hata, K., Nishizawa, M., 2013. Adv. Energy Mater. 3 (1), 60–64.
Zloczewska, A., Celebanska, A., Szot, K., Tomaszewska, D., Opallo, M., Jönsson-Niedziolka, M., 2014. Biosens. Bioelectron. 54, 455–461.
Zurbuchen, A., Pfenniger, A., Stahel, A., Stoeck, C.T., Vandenberghe, S., Koch, V.M., Vogel, R., 2013. Ann. Biomed. Eng. 41 (1), 131–141.